Resonant electronic states and *I-V* curves of Fe/MgO/Fe(100) tunnel junctions

Ivan Rungger,[1] Oleg Mryasov,[2] and Stefano Sanvito[1]
[1]*School of Physics and CRANN, Trinity College, Dublin 2, Ireland*
[2]*Seagate Research, Pittsburgh, Pennsylvania 15222, USA*
(Received 2 December 2008; published 13 March 2009)

The bias dependence of the tunnel magnetoresistance (TMR) of Fe/MgO/Fe tunnel junctions is investigated theoretically with a fully self-consistent scheme that combines the nonequilibrium Green's-function method with density-functional theory. At voltages smaller than 20 mV the *I-V* characteristics and the TMR are dominated by resonant transport through narrow interface states in the minority-spin band. In the parallel configuration this contribution is quenched by a voltage comparable to the energy width of the interface state, whereas it persists at all voltages in the antiparallel configuration. At higher bias the transport is mainly determined by the relative positions of the Δ_1 band edges in the two Fe electrodes, which causes a decrease in the TMR.

DOI: 10.1103/PhysRevB.79.094414 PACS number(s): 75.47.Jn, 73.20.−r, 73.40.Gk

I. INTRODUCTION

Modern magnetic sensors, such as read heads for hard disk drives, are based on the tunnel magnetoresistance (TMR) effect. This is the drop in resistance of a magnetic tunnel junction (MTJ) formed by two magnetic layers when the mutual alignment of their magnetization vectors changes from antiparallel (AP) to parallel (P). The TMR magnitude is given by $\mathrm{TMR}=[I_P-I_{AP}]/I_{AP}$, with $I_\alpha(V)$ being the current at the voltage V for the α configuration (P or AP). Huge TMR ratios have been recently achieved in epitaxial, all crystalline Fe/MgO (Ref. 1) and CoFeB/MgO (Ref. 2) MTJs, reaching up to 500% at room temperature and 1010% at 5 K.[3] These large values of TMR are broadly attributed to the phase-coherent and transverse momentum-conserving transport. The TMR thus is governed not only by the spin polarization of the electrode density of states (DOS), but also by the details of the wave functions matching across the barrier. Magnetic transition metals with bcc crystal structure (Fe) possess a high transmission Δ_1 band, which decays slowly across the MgO barrier.[4] This is fractionally filled for majority spins ($\uparrow$) and empty for minority spins ($\downarrow$). Since these bands dominate the tunneling current, bcc transition metals with MgO barrier effectively behave as half-metals, and the TMR is expected to be very large.[4,5]

Another important, but much less investigated aspect, is the relation between electronic states and the *I-V* characteristics in these highly crystalline MTJs. Interfacial states and details of the Fe band structure, otherwise washed out by disorder, play an important role in the transport and indeed can be identified through the *I-V* curves and its derivatives $[G(V)=dI/dV$ and $S(V)=d^2I/dV^2]$. For instance, high-quality conventional MTJs (2–3 nm MgO thickness) show a pronounced broad peak on the $S(V)$ curve at about 1 V for the AP and a number of small peaks at lower voltages in the P configuration.[6,7] Combined with a quantitative theory these measurements can provide a wealth of information and help on the level of device design. We note that very thin MTJs, with a MgO thickness of about 1 nm, have to be used for ultrahigh recording density (>500 Gbit/in.^{2}) hard disc drive readers.[8] Remarkably, at these small MgO thicknesses, the growth mode of the Fe/MgO/Fe stack changes.[7]

We investigate theoretically the *I-V* characteristics of perfectly crystalline Fe/MgO MTJs and demonstrate that its features originate from the sweeping of the Δ_1 band edges and of interface states across the bias window. These generic features are emphasized here, as they resemble closely those studied in molecular devices[9] and magnetic point contacts.[10] We investigate the ultrathin MTJ regime, with the goal to provide a solid basis for decoding future *I-V* measurements of $\lesssim$1-nm-thick MgO barriers, in terms of their relation to the underlying electronic structure and possibly growth defects.

II. SYSTEM SETUP AND METHODOLOGY

Calculations are performed using SMEAGOL,[11] which combines the nonequilibrium Green's-function method with density-functional theory (DFT).[12] The total transmission coefficient $T(E;V)$ is self-consistently evaluated at finite bias and integrated to give the spin current;

$$I^\sigma(V)=\frac{e}{h}\int dE\, T^\sigma(E;V)[f_+-f_-]. \tag{1}$$

Here σ is the spin index $(\uparrow,\downarrow)$ and $f_\pm$ is the Fermi function calculated at $(E-E_F\mp eV/2)/k_B\tau$with E_F as the Fe Fermi energy, k_B as the Boltzmann constant, and τ as the electronic temperature. Translational invariance allows us to write $T^\sigma(E;V)=\frac{1}{\Omega_k}\int T^\sigma(E,\mathbf{k}_\perp;V)d\mathbf{k}_\perp$, where the integral runs over the two-dimensional Brillouin zone perpendicular to the transport direction with area Ω_k. Large $\mathbf{k}_\perp$-point samplings are necessary to converge $T(E;V)$, so that an extremely stable numerical algorithm is needed.[13]

We consider a MTJ oriented along the Fe(100) direction and formed by four MgO monolayers (~1.1 nm long). The atomic coordinates are those from Ref. 14, which have been optimized by high-accuracy plane-wave calculations. The unit cell used for the transport contains also eight Fe atomic layers on each side of the MgO barrier, which are enough to screen the charge density from the interface. A 7×7 $\mathbf{k}_\perp$-point mesh converges the charge density, but a 100

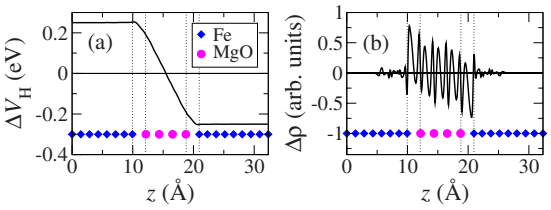

FIG. 1. (Color online) (a) Planar average ΔV_H of the difference between the Hartree potential at 0.5 V and the one at zero bias. (b) Planar average $\Delta\rho$ of the difference between the charge density at 0.5 V and the one at zero bias. The diamonds and dots indicate the location of the Fe and MgO layers.

$\times 100$ mesh is used for evaluating $T(E;V)$. The basis set employed is single ζ for the Fe p and d orbitals, while double ζ is used for all other orbitals.[12] The local-density approximation (LDA) is adopted throughout and we use a real-space mesh cutoff of 600 Ry and τ=300 K.

First, we look at the electrostatic Hartree potential drop across the junction. In Fig. 1(a) we show the difference ΔV_H between the planar average of the self-consistent Hartree potential at a finite bias and that at zero bias along the junction stack (z axis). ΔV_H is flat in the electrodes and decays linearly in MgO, demonstrating that the usual approximation of shifting rigidly the electronic structure of the electrodes and then applying a linear potential drop across the barrier[15] is well justified. In Fig. 1(b) we also show the difference $\Delta\rho$ between the planar average of the self-consistent charge density at a finite bias and at zero bias, so that $\Delta\rho(z) \propto -d^2\Delta V_H(z)/dz^2$. At all voltages we find $\Delta\rho(z)$ increasing linearly with V and charge accumulating at the extremal layers of the electrodes just before MgO. Inside the MgO $\Delta\rho(z)$ oscillates due to the electric-field-induced polarization. This is confirmed by a DFT calculation for an isolated MgO slab of the same thickness in an equivalent electric field, which shows analogous oscillations.

III. BIAS-DEPENDENT TRANSMISSION

We start our analysis of the transport properties by presenting $T(E;V)$ (Fig. 2). Three main features appear in the V=0 transmission coefficient: ① a sharp increase (note the logarithmic scale) in transmission at around −1 eV for the ↑ spins in the P configuration; ② a similar, although smoother increase above +1 eV for the ↓ spin in the P configuration and for the AP configuration; and ③ a sharp resonance at E_F for the ↓ spins in the P configuration, which is still visible in the AP configuration.

The first two features are associated with the Δ_1 band edges, respectively, for the ↑ and ↓ spins, as it can be clearly seen in Fig. 3. Note also that these band edges coincide with energy regions where the average number of Fe channels per $\mathbf{k}_\perp$ point n_c is maximized [Fig. 3(c)]. Since these are a feature of the electronic structure of Fe alone, their position as a function of bias is set by the quasi-Fermi energies, $E_F \pm eV/2$, of the two electrodes. For instance the sharp increase in $T^{\uparrow}(E;V)$ in the P configuration ① moves to −0.75 and −0.25 eV, respectively, for voltages of 0.5 and 1.5 V,

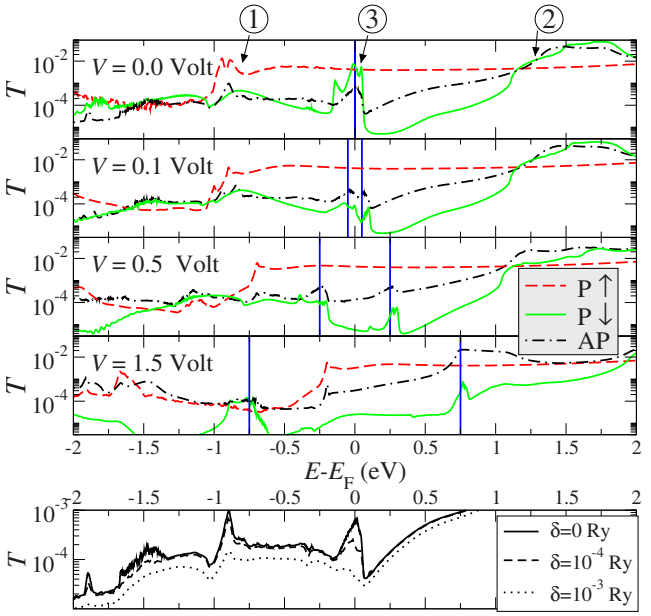

FIG. 2. (Color online) Transmission coefficient $T(E;V)$ as a function of energy E and for different biases V. The vertical lines are placed at $E=E_F \pm eV/2$ and enclose the bias window. The dashed (solid) line is for the ↑ (↓) spin band in the P configuration, while the dashed-dotted line is for the AP configuration. The lowest panel is $T(E;0)$ for the AP configuration and different broadening δ.

following the $\Delta_1^{\uparrow}$ band edge of the left lead. In the same way the broad peak in both P and AP at about 1.5 eV above E_F ② splits into two broad subpeaks, separated by eV. Note however that whereas the height of the peak is roughly constant for the AP configuration, in the P configuration the subpeak entering the bias window shrinks drastically.

In contrast the peak in transmission at E_F for the ↓ spins in the P configuration and in the AP configuration cannot be associated with leads band edges but instead originates from a narrow interface state in the minority band.[4,16–18] This is spatially localized at the interface between Fe and MgO and it is resonating at E_F. A comparison between the bulk Fe DOS and the DOS for the interface Fe layer [Figs. 3(d) and 3(e)] indicates the surface state for ↓ spins at E_F.[4] The dy-

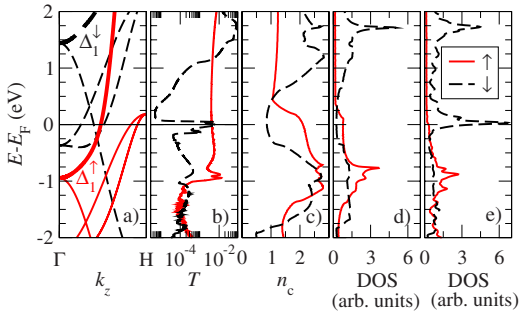

FIG. 3. (Color online) (a) Bulk Fe band structure along the Γ $\rightarrow H$ direction (the bands with Δ_1 symmetry are emphasized), (b) $T(E;0)$ in the P configuration, (c) average number of channels per $\mathbf{k}_\perp$ point for bulk Fe, n_c, (d) bulk Fe DOS, and (e) interface Fe-layer DOS. Note that the Δ_1 band edges coincide with a sharp increase in the transmission coefficient $T(E;0)$ and with a large n_c.

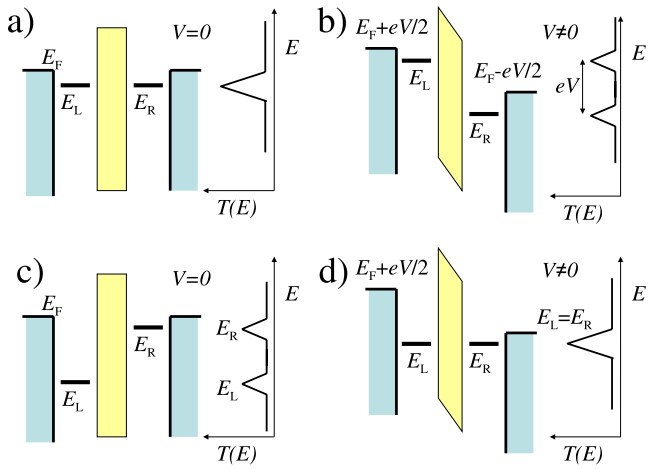

FIG. 4. (Color online) Schematic representation of the bias dependence of surface states localized at the interfaces between the magnetic electrodes and the tunnel barrier. (a) and (b) are for the left (L) and right (R) interface states having the same energy and therefore resonating at $V=0$; (c) and (d) are for the L and R interface states not resonating at zero bias.

namics of such a interface state under bias can be understood from the cartoon of Fig. 4.

Consider the panels (a) and (b) where two identical interface states are localized on either side of the tunnel barrier. This is the situation encountered here for the ↓ spins. The transport is then resonating across the barrier at the interface state energy $E_R=E_L$. In the case considered here the resonance energy is close to E_F.

Since in general the state is coupled more strongly to one of the electrodes, it will trace closely its quasi-Fermi energy. For instance for positive bias and a interface state localized on the left-hand (right-hand) side of the junction [Fig. 4(b)] we obtain $E_L(V)=E_L(0)+eV/2$ $[E_R(V)=E_R(0)-eV/2]$. This brings the states on either side of the junction out of resonance and generally suppresses the transmission. Thus the peak in $T(E;0)$, originating from a resonating interface state across the barrier, will evolve into two smaller peaks separated by an energy eV. Indeed this is the behavior observed in Fig. 2. For instance the two peaks centered at E_F are separated by 0.5 and 1.5 eV, respectively, for voltages of 0.5 and 1.5 V. In the AP configuration this situation is found at any bias since the spin ↓ interface state is always present on one side of the junction only.

A second possible situation is when the interface states on the left-hand and right-hand sides of the tunnel junction have a different origin and are placed at a different energy. In this case we do not expect zero-bias resonance; however, there will be a critical voltage at which the resonant condition is met. In this case we expect the rise of a large peak in the transmission coefficient at a bias $eV=E_L(0)-E_R(0)$. This situation has never been encountered for the symmetric MTJ investigated here, but it is likely to be the most typical case in real junctions.

IV. BIAS-DEPENDENT CURRENT AND TMR

We now move to analyzing the *I-V* characteristic and the TMR [Figs. 5 and 6], starting from the low-bias region (V

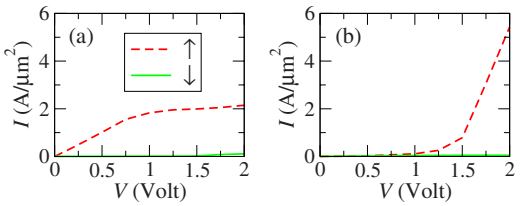

FIG. 5. (Color online) Spin-polarized current I as function of voltage V for (a) P and (b) AP alignments. Dashed lines are for the ↑ current and solid lines are for the ↓ current.

<0.4 V). The most apparent feature in this bias range is a sharp reduction in the TMR from its zero-bias value followed by a rapid increase which peaks at $V\approx 0.3$ V. The sharp reduction can be associated with a decrease in the P↓ current originating from the loss of the interface state resonant condition at $V\approx 20$ mV, a bias which roughly corresponds to the linewidth of the interface state. For $V<20$ mV the P current is shared by the two spin species, while for $V>20$ mV the ↑ component dominates. Such a reduction in the P↓ component at the bias corresponding to the resonant condition loss can be clearly observed in the $S(V)$ plot of Fig. 6(c). As the bias further increases the conductance in the P configuration is approximately constant. In contrast the conductance of the AP configuration is reduced for V between 0.1 and 0.3 V, and this behavior results in an increase in the TMR with the broad peak at 0.3 V.

The high-bias region is characterized by a decrease in the conductance in the P configuration at around 1 V and a dramatic increase in the AP current for $V>1.5$ V. This produces a strong reduction in the TMR with bias and an almost complete suppression for $V>1.5$ V. In fact at about 1.75 V the TMR becomes negative. Such a voltage range should be put in comparison with the band offset. In our LDA calculations E_F for Fe is positioned ~1.8 eV below the MgO conduction-band minimum and ~3.0 eV above the valence-

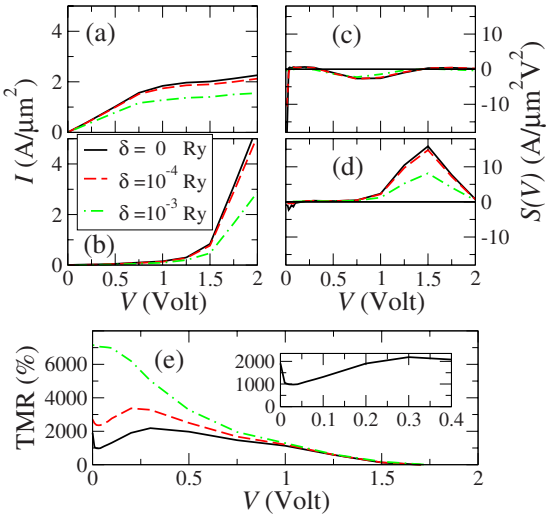

FIG. 6. (Color online) Current I, $S(V)$, and TMR as functions of voltage V for different values of the imaginary part of the energy δ: (a) *I-V* for P, (b) *I-V* for AP, (c) $S(V)$ for P, (d) $S(V)$ for AP, and (e) TMR. In the inset of panel (e) we show the TMR in the low-bias region for $\delta=0$.

band maximum. This means that voltages on the order of 1.5 V are still rather far from those needed for tunneling across a reduced barrier.

The high-bias behavior is dominated by the relative energy shift with bias of the Fe Δ_1^σ states. The origin of the reduction in the conductance in the P configuration for $V>1$ V is that once the $\Delta_1^\uparrow$ band edge of the left lead enters the bias window, the high-transmission region only extends over part of such window (Fig. 2), so that the increase in the current with bias is reduced by a factor of about 2. Note that the current in $\downarrow$ is negligible [Fig. 5(a)]. The broad peak of the $\downarrow$ transmission at about 1.5 eV above the Fermi energy, related to the $\Delta_1^\downarrow$ band edge, never contributes significantly to the current in the P configuration. The reason is that whereas for positive bias the $\Delta_1^\downarrow$ band edge of the right lead enters the bias window, the one on the left lead moves away from the bias window, so that the peak shrinks as bias is applied. The general evolution with bias of this transmission peak resembles the one of the surface states schematically shown in Figs. 4(a) and 4(b). In the AP configuration however this peak does contribute to the current since electrons belonging to the $\Delta_1^\downarrow$ band in the right lead that are inside the bias window can tunnel into the $\Delta_1^\uparrow$ bands of the left lead. This leads to an increase in the $\uparrow$ conductance once the $\Delta_1^\downarrow$ band edge moves into the bias window, resulting in a drastic increase in the AP current at $V>1.5$ V. In the same way as for P alignment, also for the AP configuration the $\downarrow$ current is negligible at high bias (Fig. 5). We note that our results in the high-bias region are in contrast with those in Ref. 19, in which a rapid increase in the conductance is found also for the P configuration.

It is also interesting to comment on the $S(V)$ plots [Figs. 6(c) and 6(d)]. For both the magnetic configurations one can observe a peaked structure. This is observed also experimentally[6] and attributed to resonances in the transmission of both inelastic and elastic origins. At the qualitative level this interpretation is confirmed by our results in the low-bias region, where the interface states determine the behavior of the *I-V*. The actual position of the peaks however depends on the atomic details of the two interfaces and we do not expect agreement. The high-bias region however is more problematic. In particular we note that our *I-V* for the P configuration does not increase as rapidly as that found in typical experiments. One possible explanation for such difference is that the MgO barrier calculated here is very thin and the current consequently is already large at small bias. Another reason could be the presence of defects at the interface and in the MgO in experiments. The most prominent feature in the $S(V)$ curves is the large broad peak at about 1.5 V, found only in the AP configuration and caused by the broad interface states associated to the $\Delta_1^\downarrow$ band edge at the Γ point. In experiments such a peak in the AP configuration only is indeed found at about 1 V.[6,7] We note that for the *I-V* curves calculated in Ref. 19 a corresponding peak in $S(V)$ would appear also in the P configuration.

Finally we investigate the effect of generic disorder, motivated by observations.[7] This is modeled at a simple level by adding a small imaginary part δ to the energy when calculating $T(E;V)$; i.e., it corresponds to a uniform level broadening.[18] The effects of such addition on the *I-V*, $S(V)$, and TMR are shown in Fig. 6, while those on $T(E;0)$ for the AP configuration are shown in Fig. 2. Figure 2 clearly shows that increasing δ results in a gradual suppression of the $T(E;0)$ resonance at E_F. For $\delta=10^{-4}$ Ry the peak is still clearly visible and only for $\delta=10^{-3}$ Ry it completely disappears. As a result the TMR at low bias largely increases and the nonmonotonic behavior for $V<0.4$ V is suppressed. In contrast the high-bias region is barely affected by δ. These results, although indicative of the effects of disorder on the TMR, should be taken with caution. The broadening δ introduces unstructured disorder, and the transmission of all the spin channels is equally reduced. In reality one may expect the transmission to either increase or decrease depending on the type of scattering center, which in general will act differently on the different spin channels. This will in general result in an enhancement of the current in the AP alignment, causing a reduction in the TMR.

V. CONCLUSIONS

In conclusion, we investigated the bias dependence of the TMR of an epitaxial Fe/MgO/Fe tunnel junction. We identify two different bias regions, which are affected by two types of electronic resonances: (i) interface resonance states and (ii) band edges. The low-bias region is characterized by a nonmonotonic behavior of the TMR caused by resonant scattering across the barrier due to the highly localized interface states. In the high-bias region ($V>0.4$ V) the TMR decreases monotonically, mainly due to band-edge states. We have also shown how disorder can suppress the transport through interface states and smoothens the TMR.

ACKNOWLEDGMENTS

This work is sponsored by Science Foundation of Ireland (Grants No. 07/IN.1/I945 and No. 07/RFP/PHYF235) and by Seagate. Computational resources have been provided by TCHPC and ICHEC. O.M. acknowledges the Science Foundation of Ireland for support during his stay at Trinity College (Walton program).

[1] S. Yuasa, T. Nagahama, A. Fukushima, Y. Suzuki, and K. Ando, Nature Mater. **3**, 868 (2004).
[2] S. S. P. Parkin, C. Kaiser, A. Panchula, P. M. Rice, B. Hughes, M. Samant, and S.-H. Yang, Nature Mater. **3**, 862 (2004).
[3] Y. M. Lee, J. Hayakawa, S. Ikeda, F. Matsukura, and H. Ohno, Appl. Phys. Lett. **90**, 212507 (2007).
[4] W. H. Butler, X.-G. Zhang, T. C. Schulthess, and J. M. MacLaren, Phys. Rev. B **63**, 054416 (2001).
[5] J. Mathon and A. Umerski, Phys. Rev. B **63**, 220403(R) (2001).
[6] Y. Ando, T. Miyakoshi, M. Oogane, T. Miyazaki, H. Kubota, K.

Ando, and S. Yuasa, Appl. Phys. Lett. **87**, 142502 (2005).
[7] P. J. Zermatten, G. Gaudin, G. Maris, M. Miron, A. Schuhl, C. Tiusan, F. Greullet, and M. Hehn, Phys. Rev. B **78**, 033301 (2008), and references therein.
[8] S. Yuasa and D. D. Djayaprawira, J. Phys. D **40**, R337 (2007).
[9] A. R. Rocha, V. M. Garcia-Suarez, S. Bailey, C. Lambert, J. Ferrer, and S. Sanvito, Nature Mater. **4**, 335 (2005).
[10] A. R. Rocha and S. Sanvito, Phys. Rev. B **70**, 094406 (2004).
[11] A. R. Rocha, V. M. Garcia-Suarez, S. Bailey, C. Lambert, J. Ferrer, and S. Sanvito, Phys. Rev. B **73**, 085414 (2006).
[12] J. M. Soler, E. Artacho, J. D. Gale, A. Garcia, J. Junquera, P. Ordejon, and D. Sanchez-Portal, J. Phys.: Condens. Matter **14**, 2745 (2002).
[13] I. Rungger and S. Sanvito, Phys. Rev. B **78**, 035407 (2008).
[14] D. Wortmann, G. Bihlmayer, and S. Blügel, J. Phys.: Condens. Matter **16**, S5819 (2004).
[15] C. Heiliger, P. Zahn, B. Yu. Yavorsky, and I. Mertig, Phys. Rev. B **73**, 214441 (2006).
[16] O. Wunnicke, N. Papanikolaou, R. Zeller, P. H. Dederichs, V. Drchal, and J. Kudrnovský, Phys. Rev. B **65**, 064425 (2002).
[17] I. Rungger, A. R. Rocha, O. Mryasov, O. Heinonen, and S. Sanvito, J. Magn. Magn. Mater. **316**, 481 (2007).
[18] K. D. Belashchenko, J. Velev, and E. Y. Tsymbal, Phys. Rev. B **72**, 140404(R) (2005).
[19] D. Waldron, L. Liu, and H. Guo, Nanotechnology **18**, 424026 (2007).